Viscous evolution of the rapidity distribution of matter created in relativistic heavy-ion collisions

Piotr Bożek[1,2,*]
[1]*Institute of Physics, Rzeszów University, PL-35959 Rzeszów, Poland*
[2]*H. Niewodniczański Institute of Nuclear Physics, PL-31342 Kraków, Poland*
(Received 20 December 2007; revised manuscript received 28 February 2008; published 31 March 2008)

The longitudinal hydrodynamic expansion of the fluid created in relativistic heavy-ion collisions is considered taking into account shear viscosity. We consider the dynamics of a non-boost-invariant energy density of the fluid in 1+1 dimensions, using the proper time and the space-time rapidity. Both a nonvanishing viscosity and a soft equation of state make the final particle distributions in rapidity narrower. The width of the initial Gaussian rapidity distribution and its central energy density are fitted to reproduce the rapidity distributions of pions and kaons as measured by the BRAHMS Collaboration. The presence of viscosity has dramatic consequences on the value of the initial energy density. Dissipative processes and the reduction of the longitudinal work due to the shear viscosity increase the total entropy and the particle multiplicity at central rapidities. Viscous corrections make the longitudinal velocity of the fluid stay close to the Bjorken scaling flow $v_z = z/t$ through the evolution.

DOI: 10.1103/PhysRevC.77.034911 PACS number(s): 25.75.Dw, 25.75.Ld

I. INTRODUCTION

Properties of hot and dense strongly interacting matter can be studied in ultrarelativistic nuclear collisions. The modeling of the evolution of the dense collective phase is most commonly undertaken within the framework of the relativistic fluid dynamics [1–3]. Clear evidence of the collective behavior of the system created in a collision is given by the observation of a substantial transverse elliptic flow of the produced particles. Collective flow arises naturally during a hydrodynamic evolution. In ultrarelativistic heavy-ion collisions, the movement of the matter at the initial stage is dominated by the expansion in the longitudinal direction. Most of the experimental data at the BNL Relativistic Heavy-Ion Collider (RHIC) are restricted to the central rapidity region. Therefore, hydrodynamic models often assume a simplified geometry of the fireball with a Bjorken boost-invariant flow in the longitudinal direction and concentrate on the dynamics in the transverse directions with azimuthal symmetry for central collisions [4–6] or azimuthally asymmetric geometry for collisions of nuclei at nonzero impact parameters [7–10]. Only a few calculations consider a fully three-dimensional evolution of the fluid [11–13]. Results of the hydrodynamic evolution are sensitive to the chosen equation of state (EOS). Values of the Hanbury-Brown-Twiss (HBT) radii observed at RHIC [14] seem to exclude equations of state with a strong first-order phase transition or even with a more prominent soft point. The hydrodynamic evolution depends on the initial temperature and its profile, on the chosen EOS, and on the freeze-out temperature. Particles emitted at the hydrodynamic freeze-out can still rescatter, which modifies somewhat their spectra and elliptic flow [10,15–17].

Instead of a fully three-dimensional calculation, only the longitudinal expansion of the matter created in a collision can be considered [4,18]. Recently the rapidity distributions of pions and kaons produced in $\sqrt{s} = 200A$ GeV Au-Au collisions measured by the BRAHMS Collaboration [19] have been analyzed in a 1+1 dimensional (in proper time and space-time rapidity) hydrodynamic model [20]. The final rapidity distribution of mesons obtained in this simplified model has been found to be sensitive to the initial energy density distribution in rapidity and to the chosen EOS. Experimental data indicate that the boost-invariant Bjorken scaling solution is not realized at RHIC energies. Results of the 1+1 dimensional longitudinal fluid dynamics for the meson rapidity distributions favor a soft EOS and a narrow Gaussian initial energy density distribution in the space-time rapidity [20].

The analysis of the elliptic flow in the momentum distribution of particles as a function of the initial eccentricity of the source points to the possibility of a noticeable effect of the shear viscosity of the fluid [21,22]. Quantitative studies have to take into account many effects, initial conditions, the equation of state, the freeze-out temperature, and possible final rescattering; therefore, estimates of the viscosity coefficient are still under debate [23,24]. Theoretical estimates of the ratio of the shear viscosity coefficient η to the entropy density s range from a conjectured lower bound $\eta/s = 1/4\pi$ [25] to $\eta \simeq s$ [26,27].

The role of the shear viscosity in the dynamics is most important during the early evolution of the system, when the velocity gradients are the largest. Gradients of the Bjorken flow give rise to corrections of the pressure tensor in the fluid. The transverse pressure increases, and the fluid expands faster in the transverse directions; this leads to stronger transverse flow and to the saturation of the elliptic flow [23,28–33]. All recent calculations using viscous relativistic hydrodynamics assume boost-invariant Bjorken flow in the longitudinal direction and study the transverse development of the fluid in azimuthally symmetric or asymmetric conditions. Longitudinal pressure is reduced, and hence so is the longitudinal flow of the fluid. The fluid cools slower, at least until substantial transverse flow builds up. Weaker longitudinal expansion and entropy production due to dissipative evolution require an adjustment of the initial entropy (temperature). As a result, the lifetimes of

*Piotr.Bozek@ifj.edu.pl

the plasma in the viscous and ideal fluid evolutions are similar. Finally, let us note that viscous corrections to the distribution functions at the freeze-out modify the spectra and the HBT radii [32,34].

Enhanced transverse pressure and the resulting modification of the spectra at central rapidities raise the question of possible modifications of the fluid dynamics in the longitudinal direction due to viscosity. Since the boost-invariant scaling solution is not applicable at RHIC energies, the quantitative description of the energy flow and entropy production in the fireball should take into account a fully three-dimensional geometry. Such a task within the dissipative fluid dynamics has not been accomplished yet. In the following we consider a simpler problem of the evolution of a longitudinally expanding non-boost-invariant fluid with viscosity. The flow is directed only in the longitudinal direction. The flow velocity, the energy density, and the shear viscosity corrections depend only on the proper time and space-time rapidity. In such a framework, one expects that reduced longitudinal work in a viscous fluid generates narrower particle distributions in rapidity than in a similar evolution of an ideal fluid. The author is aware of only one two-decades old work considering this problem [35] in which first-order viscous hydrodynamics was applied. At low energies, no strong effect of viscosity on the longitudinal expansion was observed [35].

In the following we use BRAHMS data [19] to constrain meson rapidity distributions after freeze-out. Solving viscous hydrodynamics in the 1+1 longitudinal geometry and adjusting the parameters of the initial density, we find a significant reduction of the initial energy density when viscosity is taken into account. Although the values of the obtained parameters are only indicative because of the very simplified geometry, the qualitative dependence of the initial energy density on the viscosity coefficient is generic. Also the longitudinal flow is modified; viscosity reduces the flow and counteracts the acceleration due to rapidity gradients of the pressure. At the CERN Large Hadron Collider (LHC) energies, we find that the modification of the longitudinal dynamics due to shear viscosity leads to an increase of the rapidity range where the Bjorken scaling flow applies in the final state, assuming that such a Bjorken plateau is present in the initial distributions.

II. LONGITUDINAL HYDRODYNAMIC EQUATIONS WITH SHEAR VISCOSITY

We consider a baryon-free fluid with nonzero shear viscosity. The energy-momentum tensor is the sum of the ideal fluid component and the shear tensor $\pi^{\mu\nu}$

$$T^{\mu\nu} = (\epsilon + p)u^\mu u^\nu - pg^{\mu\nu} + \pi^{\mu\nu}, \tag{2.1}$$

where ϵ and p are the local energy density and pressure of the fluid,

$$\begin{aligned} u^\mu &= \gamma(1, 0, 0, v) \\ &= (\cosh Y, 0, 0, \sinh Y) \end{aligned} \tag{2.2}$$

is the four-velocity of the fluid element ($\gamma = 1/\sqrt{1-v^2}$), and $Y = \frac{1}{2}\ln(\frac{1+v}{1-v})$ is its rapidity. In the whole evolution, the velocity of the fluid is directed in the longitudinal direction; the transverse flow is neglected. The energy density and the pressure are related by the equation of state. The energy density $\epsilon(t, z)$ and the longitudinal velocity component $v(t, z)$ are functions of the time t and the beam axis coordinate z only. Instead of the time and the z coordinate, it is preferable to use the proper time $\tau = \sqrt{t^2 - z^2}$ and the space-time rapidity

$$\theta = \frac{1}{2}\ln\left(\frac{t+z}{t-z}\right). \tag{2.3}$$

Hydrodynamic equations $\partial_\mu T^{\mu\nu} = 0$ can be written as [36,37]

$$(\epsilon + p)Du^\mu = \nabla^\mu p - \Delta^\mu_\nu \nabla_\alpha \pi^{\nu\alpha} + \pi^{\mu\nu} Du_\nu \tag{2.4}$$

and

$$D\epsilon = -(\epsilon + p)\nabla_\mu u^\mu + \tfrac{1}{2}\pi^{\mu\nu}\langle\nabla_\mu u_\nu\rangle, \tag{2.5}$$

where

$$D = u^\mu \partial_\mu = \cosh(Y - \theta)\partial_\tau + \frac{\sinh(Y-\theta)}{\tau}\partial_\theta, \tag{2.6}$$

$$\langle\nabla_\mu u_\nu\rangle = \nabla_\mu u_\nu + \nabla_\nu u_\mu - \frac{2}{3}\Delta_{\mu\nu}\nabla_\alpha u^\alpha, \tag{2.7}$$

$$\begin{aligned} \nabla^\mu &= \Delta^{\mu\nu}\partial_\nu \\ &= (-\sinh Y\mathcal{K}, -\partial_x, -\partial_y, -\cosh Y\mathcal{K}), \end{aligned} \tag{2.8}$$

with $\Delta_{\mu\nu} = g_{\mu\nu} - u_\mu u_\nu$ and

$$\mathcal{K} = \sinh(Y - \theta)\partial_\tau + \frac{\cosh(Y-\theta)}{\tau}\partial_\theta. \tag{2.9}$$

The equations of second-order viscous hydrodynamics (2.4) and (2.5) are supplemented with a dynamic equation for the stress tensor [29,34,37–40]

$$\tau_\pi \Delta^\mu_\alpha \Delta^\nu_\beta \pi^{\alpha\beta} + \pi^{\mu\nu} = \eta\langle\nabla^\mu u^\nu\rangle - 2\tau_\pi \pi^{\alpha(\mu}\omega^{\nu)}_\alpha, \tag{2.10}$$

where η is the shear viscosity coefficient and τ_π is the relaxation time of the stress tensor. The above equation defines the stress tensor $\pi^{\mu\nu}$, i.e., the traceless and orthogonal to u^μ deviation of the energy-momentum tensor from the one of the ideal fluid. $\omega^{\mu\nu} = \Delta^{\mu\alpha}\Delta^{\nu\beta}(\partial_\alpha u_\beta - \partial_\beta u_\alpha)$ is the vorticity of the fluid; it is zero for the longitudinal flow considered here. The relaxation time and the viscosity coefficient can be estimated from microscopic models, considering equilibration processes [25–27,41]. In this work, we take several values for the ratio of the viscosity coefficient to the entropy η/s, and we drop viscosity effects for temperatures below 130 MeV; the relaxation time is [26] $\tau_\pi/\eta = 6/Ts$, unless specified otherwise (T is the local temperature). For short relaxation times, the stress tensor relaxes fast and stays close to the Navier-Stokes value $\pi^{\mu\nu} = \eta\langle\nabla^\mu u^\nu\rangle$. The dependence on the initial value of the stress tensor and on the relaxation time is discussed in Sec. VI.

For a fluid expanding only in the longitudinal direction, with the energy density and the velocity constant in the transverse plane, the stress tensor can be written using one scalar function Π

$$\pi^{\mu\nu} = \begin{pmatrix} -\sinh^2 Y & 0 & 0 & -\sinh Y\cosh Y \\ 0 & \frac{1}{2} & 0 & 0 \\ 0 & 0 & \frac{1}{2} & 0 \\ -\sinh Y\cosh Y & 0 & 0 & -\cosh^2 Y \end{pmatrix}\Pi. \tag{2.11}$$

Such a simple form of the shear tensor is due to the assumed form of the flow, in the longitudinal direction only and independent of the transverse coordinates. In general the shear tensor has *five* independent components. In the considered 1+1 dimensional geometry, viscous hydrodynamic equations take the form

$$\begin{aligned}(\epsilon + p)DY &= -\mathcal{K}p + \Pi DY + \mathcal{K}\Pi,\\ D\epsilon &= (\epsilon + p)\mathcal{K}Y - \Pi\mathcal{K}Y,\\ D\Pi &= \left(\tfrac{4}{3}\eta\mathcal{K}Y - \Pi\right)/\tau_\pi.\end{aligned} \tag{2.12}$$

The above equations are solved numerically in the τ-θ plane, starting from some energy density $\epsilon(\tau_0, \theta)$ at the initial proper time of the evolution, $\tau_0 = 1.0$ fm/c. For the initial fluid rapidity, we always take the Bjorken flow

$$Y(\tau_0, \theta) = \theta. \tag{2.13}$$

Assuming boost invariance, i.e.,

$$Y(\tau, \theta) = \theta, \quad \epsilon(\tau, \theta) = \epsilon(\tau), \quad p(\tau, \theta) = p(\tau), \tag{2.14}$$

the hydrodynamic equations simplify to [37,38]

$$\begin{aligned}\frac{d\epsilon}{d\tau} &= -\frac{\epsilon + p - \Pi}{\tau},\\ \frac{d\Pi}{d\tau} &= \frac{(4\eta)/(3\tau) - \Pi}{\tau_\pi}.\end{aligned} \tag{2.15}$$

III. EQUATION OF STATE

The EOS determines the evolution of the fireball. In the following we take a parametrization of the EOS proposed by Chojnacki and Florkowski [42]. It is an interpolation of the lattice data at temperatures above $T_c = 170$ MeV and of an EOS of noninteracting hadrons at lower temperatures. The two limiting formulas are joined smoothly with only a slight softening of the EOS around the critical temperature (Fig. 1). This minimally softened, realistic EOS has proved to be suitable for describing the transverse expansion of the fluid and the buildup of the elliptic flow, and it gives reasonable HBT radii [42,43].

In this section, we consider the hydrodynamic longitudinal expansion of an ideal fluid. Equations for fluid rapidity and energy density are obtained from Eqs. (2.12) setting $\Pi = 0$. This problem has been discussed recently in the context of heavy-ion collisions at RHIC [20]. For completeness, we study the effect of the EOS we use on the longitudinal expansion. For that purpose, we compare the evolution using the EOS of Chojnacki and Florkowski with an evolution based on a relativistic gas EOS $p = \frac{1}{3}\epsilon$.

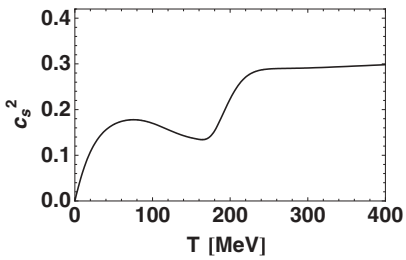

FIG. 1. Square of the velocity of sound as a function of temperature for an EOS interpolating between the hadron gas and the quark-gluon plasma expressions [42].

At the initial time $\tau_0 = 1.0$ fm/c, the energy density profile is taken as

$$\epsilon(\tau_0, \theta) = \epsilon_0 \exp(-\theta^2/(2\sigma^2)). \tag{3.1}$$

The initial energy density ϵ_0 and the width of the initial rapidity distribution σ are parameters adjusted to reproduce final meson rapidity distributions. The freeze-out takes place at the temperature $T_f = 165$ MeV; this high freeze-out temperature is the same as the chemical freeze-out temperature [44,45]. The spectrum of particles emitted with four-momentum $q^\mu = (E, q)$ is given by the Cooper-Frye formula [20,46]

$$E\frac{d^3N}{d^3q} = \frac{d^3N}{dy\, d^2q_\perp} = \frac{1}{(2\pi)^3}\int d\Sigma_\mu q^\mu f(q^\mu u_\mu), \tag{3.2}$$

$f(E) = e^{-E/T_f}$ is the thermal distribution corresponding to the Jüttner distribution in the Cooper-Frye formula (Boltzmann distribution for simplicity), and y denotes the rapidity of the emitted particle. The EOS of the fluid at the freeze-out temperature is the same as the EOS of a gas of noninteracting hadrons [42]. The continuity of the EOS should guarantee the conservation of energy and momentum; however, the approximation of the thermal Fermi and Bose distributions of hadrons by the Boltzmann distribution breaks these relations to some extend. Energy conservation is even more severely broken for the illustrative calculations of this section using a constant sound velocity ($p = \epsilon/3$) [47]. Also, the assumption that particles after freeze-out follow the Jüttner distribution is an approximation, the quality of which depends on the time extent of the freeze-out process [48]. Such deviations from thermal distributions could have noticeable consequences on some observables [49]. Since in the limit of massless particles the rapidity distribution of particles emitted from a source does not depend on the form of the momentum distribution, we expect that also for massive particles the rapidity distribution is not very sensitive to these effects.

The element of the hypersurface of constant freeze-out temperature is $d\Sigma^\mu = S(\tau'(\theta)\sinh\theta + \tau(\theta)\cosh\theta, 0, 0, \tau'(\theta)\cosh\theta - \tau(\theta)\sinh\theta)$, where $S = \pi R_{\mathrm{Au}}^2$ is the transverse area of the fireball in central collisions and $\tau(\theta)$ is the line of constant temperature T_f in the τ-θ plane. Particle distributions in rapidity are obtained by integration over the transverse momenta $q_\perp$ in Eq. (3.2)

$$\begin{aligned}\frac{dN}{dy} = \frac{S}{4\pi^2}\int_{-\theta_{\max}}^{\theta_{\max}} &(\tau(\theta)\cosh(y-\theta) - \tau'(\theta)\sinh(y-\theta))\\ &\times (2m\xi + 2\xi^2 + m^2)\xi \exp\left(-\frac{m\cosh(y - Y_f(\theta))}{T_f}\right)d\theta,\end{aligned} \tag{3.3}$$

m is the meson mass, $Y_f(\theta) = Y(\tau(\theta), \theta)$ is the fluid rapidity at the freeze-out hypersurface, and

$$\xi = \frac{T_f}{\cosh(y - Y_f(\theta))}. \tag{3.4}$$

The expression (3.3) neglects the transverse expansion of the fluid at the freeze-out. This has only a small effect on rapidity distributions, the distributions should be narrower. Pions and kaons come to a large extent from secondary decay of resonances. The emission takes place in two stages, first an emission of a heavy resonance according to Eq. (3.3) and then the decay of the resonance into pions (kaons). The emission of resonances and their decay is also influenced by their transverse expansion. A hint of the spread in rapidity of the decay products of resonances is given by charge balance correlations [50–52]. Narrow charge balance functions indicate that decay products of a resonance are only 0.5 unit of rapidity away from the parent resonance; convoluting this distribution with the spread in rapidity of the emitted resonances, one obtains a distribution of half-width similar to that for the emission of direct pions in Eq. (3.3). Since 75% of pions come from resonances at $T_f = 165$ MeV [53], we multiply the distribution from Eq. (3.3) by a factor of 4 to account for all pions, direct and from resonance decays (the factor is 1.7 for kaons).

The parameters ϵ_0 and σ have been adjusted for the calculation using a realistic sound velocity (Fig. 1) to reproduce the width and normalization of the observed pion distribution. As a result, the final meson distributions can be made similar to the ones observed experimentally. On the other hand, when using an ultrarelativistic gas EOS ($p = \frac{1}{3}\epsilon$) one always gets a meson distribution in rapidity that is too wide. We present three calculations (for $p = \frac{1}{3}\epsilon$) with different initial widths σ and with the initial energy densities ϵ_0 adjusted to reproduce dN/dy for central rapidities only (Fig. 2 and Table I). The final meson distribution is much wider than the initial energy density distribution in all cases because of the breaking of the Bjorken scaling of the longitudinal flow, $Y(\tau, \theta) > \theta$ (Fig. 3). Fast-moving fluid elements emit mesons in the far forward and backward rapidities.

TABLE I. Parameters of the initial energy density distribution [Eq. (3.1)] for ideal fluid calculations, one using a realistic EOS and three calculations using a relativistic gas EOS. The last column shows the lifetime of the system until freeze-out.

	ϵ_0 (GeV/fm^3)	σ	$\tau(0)$ (fm/c)
EOS [42]	16.9	1.05	14.8
$p = \frac{1}{3}\epsilon$ case I	71.5	1.05	14.8
$p = \frac{1}{3}\epsilon$ case II	102	0.8	15.7
$p = \frac{1}{3}\epsilon$ case III	50.8	1.5	13.7

Concluding this section, we confirm the findings of Ref. [20]. Within the framework of 1+1 dimensional hydrodynamics, a hard EOS never works. A narrow initial distribution of the energy density in rapidity leads to a strong acceleration of the longitudinal flow; wider initial distributions are incompatible with the narrow final meson distributions. In the simple 1+1 dimensional model only by imposing a softened EOS, experimental pion and kaon distributions can be approximately reproduced. The development of transverse flow is expected to relax somewhat this constraint on the equation of state. In the following, we take the realistic EOS from Ref. [42] and study the effect of nonnegligible shear viscosity.

IV. DISSIPATIVE LONGITUDINAL EXPANSION

Following the hydrodynamic evolution with viscosity requires the solution of the coupled equations (2.12), for the fluid rapidity Y, the viscous correction Π, and the energy density ϵ. The initial conditions are given in Eqs. (3.1) and (2.13). For the initial viscous corrections, we take $\Pi(\tau_0, \theta) = p(\tau_0, \theta)$. This means that at the initial time, the effective pressure

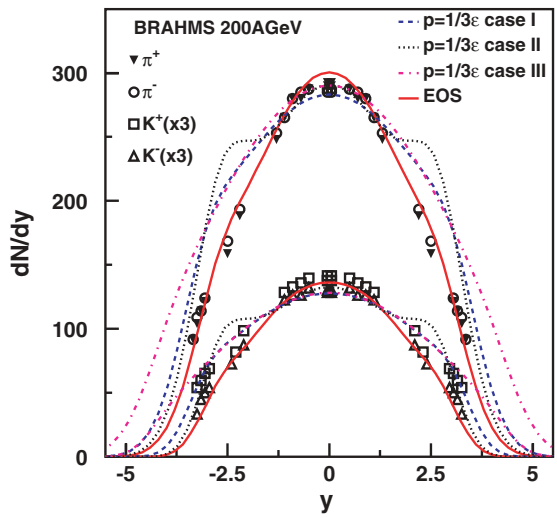

FIG. 2. (Color online) Rapidity distribution of mesons calculated using a realistic EOS (solid line) and using a relativistic gas EOS for three different initial conditions (dashed, dotted, and dashed-dotted lines), see Table I. Data are from the BRAHMS Collaboration [19].

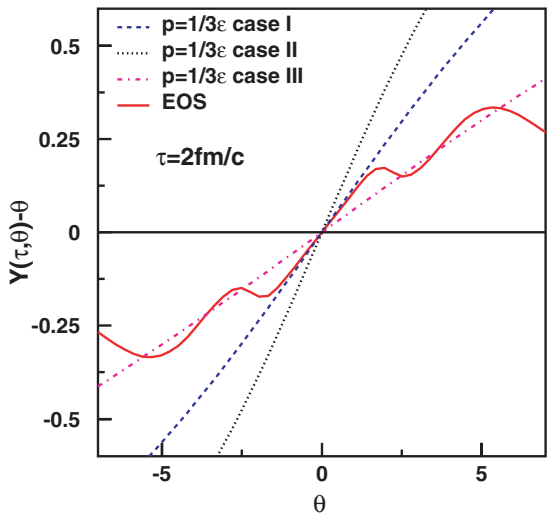

FIG. 3. (Color online) Difference between the flow rapidity of the fluid and the Bjorken value, calculated using a realistic EOS and using a relativistic gas EOS for three different initial conditions, see Table I.

is maximally anisotropic in the fluid rest frame, with zero longitudinal pressure. We vary the value of the shear viscosity coefficient η/s, and in each case we adjust the parameters of the initial energy density distribution [Eq. (3.1)] to reproduce BRAHMS data for the pion distribution in rapidity. Viscous corrections modify the momentum distribution functions in the fluid and the energy-momentum tensor. In the fluid rest frame, the pressure is anisotropic. The form of the energy-momentum tensor is not enough to fix the corresponding momentum distributions of the noninteracting gas after freeze-out. As mentioned in Sec. III, the momentum distribution after freeze-out depends on the details of the decoupling process [48]. The same is true if viscous corrections are important. The simplest formula for the momentum distribution with viscous corrections can be assumed in the form of a multiplicative correction to the Jüttner distribution [28]. We assume the same modification for all the particle species in the fluid

$$f(q) + \delta f(q) = f(q)\left(1 + \frac{q_\mu q_\nu \pi^{\mu\nu}}{2T^2(\epsilon + p)}\right). \tag{4.1}$$

The correction to the particle distribution function is proportional to the ratio of the viscous correction Π to the enthalpy $\epsilon + p$. Viscous corrections to the distribution functions at the freeze-out modify the outcome of the Cooper-Frye formula

$$\frac{dN_{\rm visc}}{dy} = \frac{dN}{dy} + \frac{d\delta N}{dy}. \tag{4.2}$$

To the expression (3.3), one has to add

$$\begin{aligned}\frac{d\delta N}{dy} = {} & \frac{S}{4\pi^2}\int_{-\theta_{\rm max}}^{\theta_{\rm max}} (\tau(\theta)\cosh(y-\theta) - \tau'(\theta)\sinh(y-\theta)) \\ & \times [12\xi^5 + 5\xi^3 m^2 + 12\xi^4 m + \xi^2 m^3 \\ & - \sinh(y - Y_f(\theta))(24\xi^5 + 12\xi^3 m^2 + 24\xi^4 m \\ & + 4\xi^2 m^3 + \xi m^4)]\frac{\Pi}{2T^2(\epsilon + p)} \\ & \times \exp\left(-\frac{m\cosh(y - Y_f(\theta))}{T_f}\right) d\theta,\end{aligned} \tag{4.3}$$

In Fig. 4 is shown the result of this procedure for the case $\eta/s = 0.2$. Again, direct meson spectra are multiplied by a factor of 4 for pions and 1.7 for kaons, to account for the expected ratio of all mesons to directly produced mesons [53], at the chosen freeze-out temperature. Pion emission at the end of the viscous hydrodynamic evolution (solid line) can be made similar as observed experimentally after tuning the parameters of the initial Gaussian energy density profile. In Fig. 4 is also shown the meson distribution obtained using the equilibrium distribution at freeze-out [Eq. (3.3), dotted line]. Deviations from the full result [Eq. (4.2)] is only noticeable at rapidities three units away from central rapidity. It can be understood as being due to an earlier freeze-out at large rapidities, which makes the relative viscous corrections

$$\frac{\Pi(\tau(\theta), \theta)}{\epsilon(\tau(\theta), \theta) + p(\tau(\theta), \theta)} \tag{4.4}$$

at freeze-out more important (Fig. 5). Modifications of the momentum distributions from viscous corrections given by equation (4.1) are know to modify particle distributions in

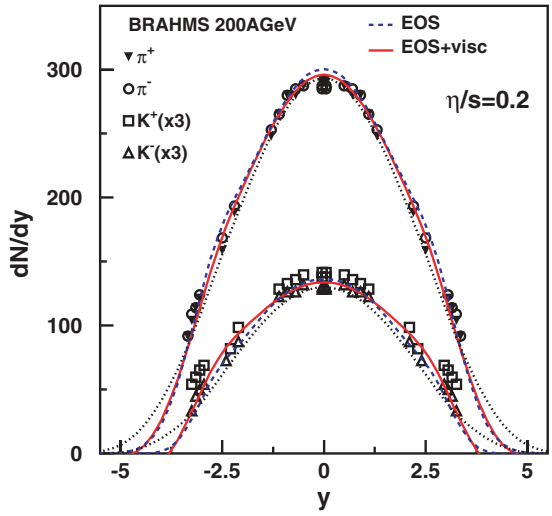

FIG. 4. (Color online) Rapidity distribution of mesons calculated using a realistic EOS and viscosity $\eta/s = 0.2$ (solid line) and using ideal fluid hydrodynamics (dashed line). The dotted line denotes the results of a viscous hydrodynamic evolution, but neglecting the viscous corrections to the particle emission at freeze-out [Eq. (4.3)]. Data are from the BRAHMS Collaboration [19].

the transverse momentum [28], the p_T spectra, the HBT radii and the elliptic flow. In our estimate, a more important effect would come from the neglected transverse expansion of the fluid than from nonequilibrium corrections in Eq. (4.3). Hopefully we find that the rapidity distribution is not sensitive to nonequilibrium, anisotropic modifications of the momentum distribution (4.1). Following the estimates of Teaney [28], only at large rapidities could one expect some corrections from the longitudinal flow with viscosity to particle spectra, elliptic flow, and HBT radii. However, at high rapidities, the 1+1 dimensional geometry assumed in the paper is questionable.

We have noticed (Sec. III) that longitudinal pressure gradients accelerate the fluid motion in the beam direction. On the other hand, viscosity reduces the longitudinal motion of the fluid and as a consequence reduces its expansion in the longitudinal direction. Shear viscosity prevents the development of large gradients of the velocity field. One can compare the rapidity of the fluid with and without shear viscosity

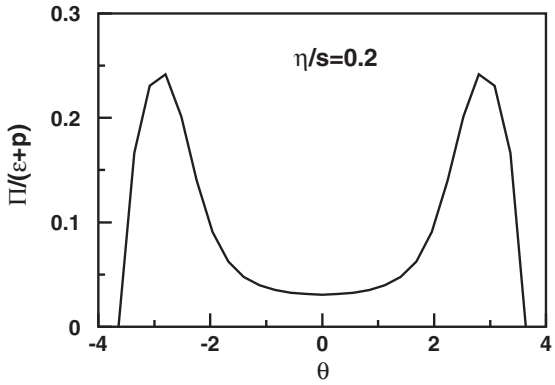

FIG. 5. Relative viscous corrections $\Pi/(\epsilon + p)$ at freeze-out as a function of space-time rapidity [Eq. (4.4)].

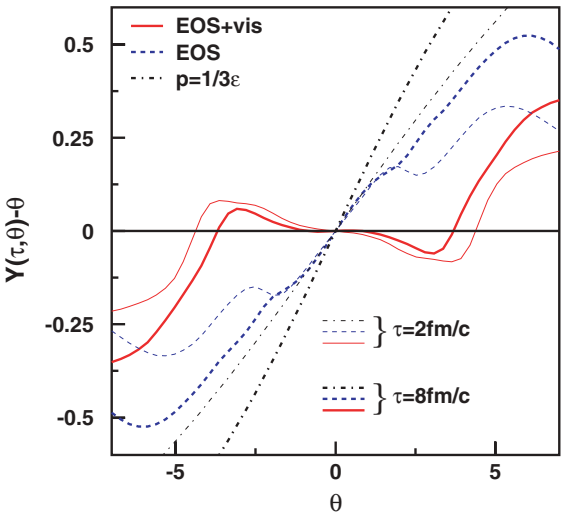

FIG. 6. (Color online) Difference between the flow rapidity of the fluid and the Bjorken value, calculated for an evolution with shear viscosity coefficient $\eta/s = 0.2$ (solid lines), for an ideal fluid with a realistic EOS (dashed lines), and using a relativistic gas EOS (case I) (dashed-dotted lines).

(Fig. 6). For $\eta/s = 0.2$, the flow stays close to the Bjorken one during a substantial part of the evolution. At the freeze-out hypersurface, the flow is still Bjorken-like for $|\theta| < 1.8$ and $\eta/s = 0.2$ (Fig. 7). The acceleration from pressure gradients and the deceleration from viscosity approximately cancel for this choice of parameters. Reduced longitudinal expansion with viscosity requires smaller initial energy densities to reproduce the final meson distributions. Table II lists the initial energy densities and widths of rapidity distributions adjusted to reproduce the observed meson distributions for several values of the shear viscosity coefficient. The shape of the

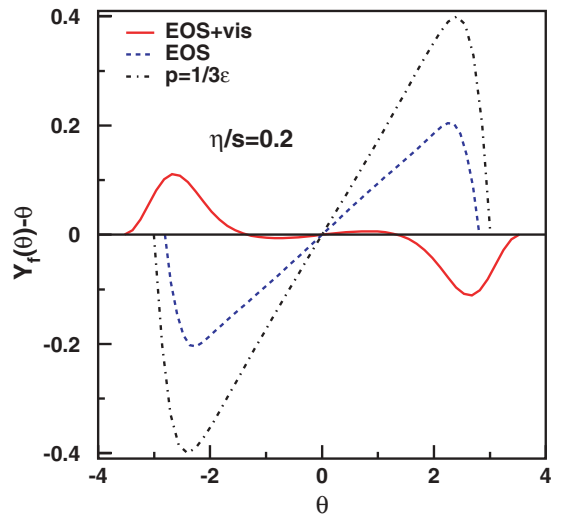

FIG. 7. (Color online) Difference between the flow rapidity of the fluid and the Bjorken value at the freeze-out hypersurface, calculated for an evolution with shear viscosity coefficient $\eta/s = 0.2$ (solid line), for an ideal fluid with a realistic EOS (dashed line), and using a relativistic gas EOS (case I) (dashed-dotted line).

TABLE II. Parameters of the initial energy density distribution of Eq. (3.1) for hydrodynamic calculations with several values of the shear viscosity coefficient. The last column shows the lifetime of the system until freeze-out.

η/s	ϵ_0 (GeV/fm^3)	σ	$\tau(0)$ (fm/c)
0	16.9	1.05	14.8
0.1	9.8	1.18	14.1
0.2	5.6	1.8	13.1
0.3	4.0	1.86	12.4

initial energy density is extremely sensitive to the dynamics of the longitudinal expansion (Fig. 8). Obviously the value of the initial energy density, or in other words the cooling rate from the longitudinal motion, is an important ingredient in the modeling of the transverse expansion of the fluid. Let us also note that when reduced initial energy densities are imposed, the lifetime of the system until freeze-out is only weakly dependent on the viscosity coefficient.

All the results presented so far are obtained using a Gaussian initial energy density profile in space-time rapidity [Eq. (3.1)], which best reproduces the observed meson distributions. In a fully three-dimensional hydrodynamic simulation, initial profiles of the energy density with a plateau in the space-time rapidity are used [13] to reproduce the experimental distributions. The difference lies in the complete treatment of the transverse expansion. A similar initial energy density profile with a plateau can be also used in the 1+1 dimensional model studied in this paper, that is,

$$\epsilon(\tau_0, \theta) = \epsilon_0 \exp(-(\theta - \sigma_p)^2 \Theta(|\theta| - \sigma_p)/2\sigma^2). \quad (4.5)$$

Using a relatively narrow plateau for central rapidities, $\sigma_p = 0.4$, one gets meson distributions compatible with the experimental data of the BRAHMS Collaboration by tuning the parameters ϵ_0 and σ of the initial distribution (Table III).

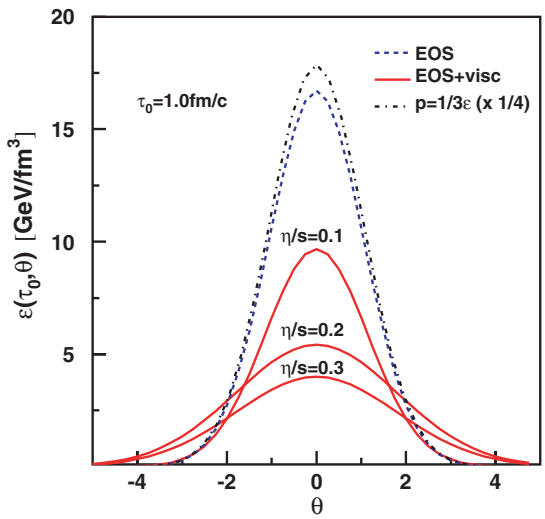

FIG. 8. (Color online) Initial energy density distribution for the ideal fluid hydrodynamic evolution with a realistic EOS (dashed line), for viscous hydrodynamic evolutions (solid lines), and for a relativistic gas EOS (case I) (dashed-dotted line).

TABLE III. Parameters of the initial energy density distribution of Eq. (4.5) for hydrodynamic calculations with several values of the shear viscosity coefficient, $\sigma_p = 0.4$. The last column shows the lifetime of the system until freeze-out.

η/s	ϵ_0 (GeV/fm^3)	σ	$\tau(0)$ (fm/c)
0	14.3	0.9	14.8
0.1	8.1	1.0	13.3
0.2	5.2	1.5	12.2
0.3	4.3	1.7	11.8

Similarly as for Gaussian initial conditions with an increasing shear viscosity coefficient, the initial energy density goes down. For $\eta/s \leqslant 0.2$, the initial energy density is smaller for the initial condition with a plateau than for the Gaussian profile. It is a sign of a slower cooling in a boost-invariant system than in a system with gradients in space-time rapidity (see Sec. V); while for $\eta/s = 0.3$, the situation is reversed. We have to realize that the extraction of the form of the initial energy density in such a simple 1+1 dimensional model is not very realistic. Nevertheless, we can conclude that it should be a relatively narrow distribution in space-time rapidity and that the initial energy density decreases with increasing shear viscosity.

V. COOLING AND ENTROPY PRODUCTION

It is instructive to compare the cooling rate in our solution and in the boost-invariant scaling solution. Finite extension in space-time rapidity makes the cooling rate faster. On the other hand, reduced velocity of sound and shear viscosity reduce the longitudinal work of the pressure and slow down the cooling. Figure 9 compares the cooling of the central region of a finite system to the cooling in the boost-invariant case [Eq. (2.15)].

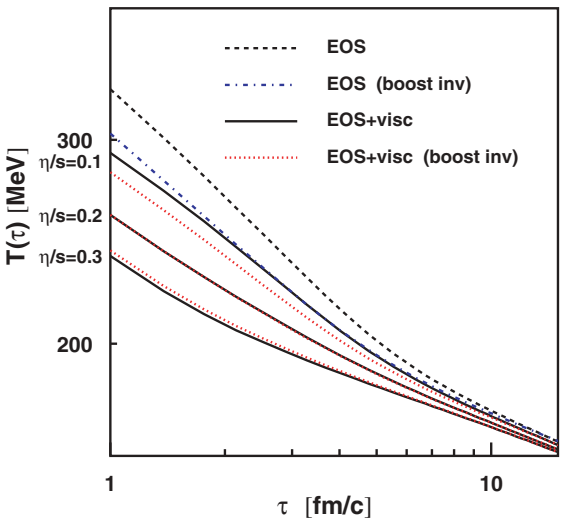

FIG. 9. (Color online) Time dependence of the temperature at the center for a longitudinally expanding ideal fluid fireball (dashed line) compared with the boost-invariant solution (dashed-dotted line). Same for the evolution with viscosities $\eta/s = 0.1, 0.2, 0.3$ (solid lines, increasing η from top to bottom), and for the boost-invariant case with viscosity (dotted lines). For $\eta/s = 0.2$, the solid and dotted curves lie on top of each other.

To compare the solution in the 1+1 dimensional system to the boost-invariant one, the initial temperatures are fixed so as to give the same lifetimes of the two systems until freeze-out. Boost-invariant solutions underestimate the values of the initial temperature (energy density) and of the cooling rate for an ideal fluid evolution. In a finite system, additional cooling appears and the longitudinal flow is stronger than the Bjorken scaling flow. As the shear viscosity coefficient increases, the velocity gradients in the dynamics are more and more constrained. The flow accelerates less. At $\eta/s = 0.2$, the effects of the viscosity and space-time rapidity gradients of the pressure counterbalance each other, and the flow is approximately Bjorken-like. With stronger viscosity $\eta/s = 0.3$, the Bjorken flow is decelerated, and the cooling is slower than for the boost-invariant solution. This means that the gradients of the viscous correction Π are larger than the gradients of the pressure itself, and the applicability of second-order viscous hydrodynamics is questionable.

Dissipative hydrodynamics conserves the total energy but produces entropy. The expression for the total energy of the system at proper time τ is

$$E(\tau) = \tau S \int_{-\infty}^{\infty} d\theta [\epsilon \cosh Y \cosh(Y - \theta) + (p - \Pi) \sinh Y \sinh(Y - \theta)]. \tag{5.1}$$

It is mainly composed of the kinetic energy of the longitudinal motion of the fluid. Small changes of the energy density at large rapidities can cause significant changes of the energy density for central rapidities. Softening of the EOS and nonzero shear viscosity modify the dynamics at large rapidities, which leads to less cooling at $\theta = 0$, while the global energy of the fireball is unchanged. Dissipative processes driving the system locally toward equilibrium produce entropy [39–41,54,55]. The total entropy of the system

$$S(\tau) = \tau S \int_{-\infty}^{\infty} d\theta \, s \cosh(Y - \theta) \tag{5.2}$$

increases with time, if shear viscosity is active (Fig. 10). Conservation of entropy given by Eq. (5.2) in the ideal fluid evolution is a good test of the quality of the numerical solution. Numerical viscosity could cause a spurious increase of the entropy for the ideal fluid. We have checked that the relative increase of the entropy in the ideal fluid evolution, due to numerical effects in the dynamics, is 2×10^{-4} after 20 fm/c. When reducing the shear viscosity coefficient, the relative entropy production smoothly decreases from about 50% at $\eta/s = 0.2$ to 0.1% for $\eta/s = 10^{-3}$. This means that the observed dissipative effects of the shear viscosity are not due to numerical inaccuracies of the solution.

The increase of the entropy at central rapidity $\tau s(\tau, \theta)$ is responsible for an increase of the particle multiplicity in the central rapidity region. Estimates of the entropy production [55] based on the boost-invariant solution [Eq. (2.15)]

$$\frac{d(\tau s)}{d\tau} = \frac{\Pi}{T} \tag{5.3}$$

are very close to the 1+1 dimensional dynamical result, which happens if the shear viscosity is strong enough to conserve the Bjorken flow in the evolution.

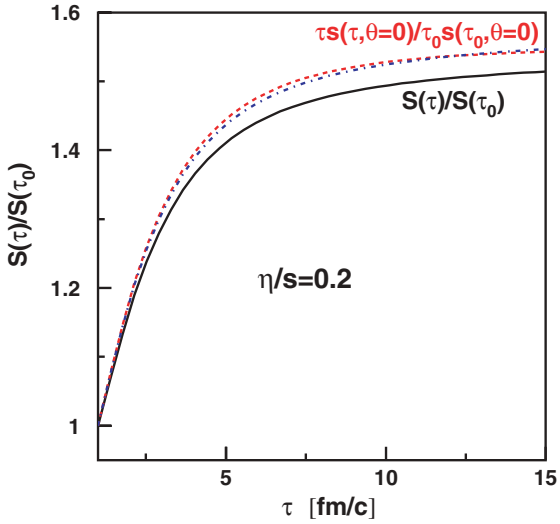

FIG. 10. (Color online) Relative entropy production in the viscous hydrodynamic evolution [Eq. (5.2)] (solid line), of the entropy density at central space-time rapidity (dashed line), and of the entropy from the boost-invariant Bjorken solution [Eq. (5.3)] (dashed-dotted line). All calculations are with $\eta/s = 0.2$.

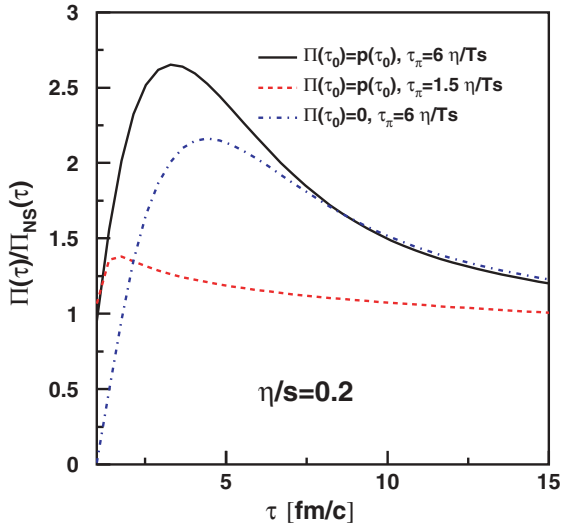

FIG. 11. (Color online) Ratio of the dynamical shear viscosity correction $\Pi(\tau)$ to the Navier-Stokes value $\Pi_{\rm NS}(\tau)$ at $\eta/s = 0.2$ for two initial conditions for the viscous corrections $\Pi(\tau_0) = p(\tau_0)$ (solid line) and for $\Pi(\tau_0) = 0$ [Eq. (6.1)] (dashed-dotted line), and for a reduced relaxation time $\tau_\pi = 1.5\eta/Ts$ (dashed line).

VI. ROLE OF THE INITIAL STRESS TENSOR

Second-order viscous hydrodynamics introduces a dynamical equation for the stress tensor. A crucial parameter is given by the relaxation time τ_π. For small relaxation times, the viscosity correction stays close to the Navier-Stokes value

$$\Pi_{\rm NS}(\tau) = \frac{4\eta}{3\tau}. \tag{6.1}$$

Such a behavior of viscous corrections has been confirmed in numerical simulations of the transverse expansion in viscous hydrodynamics with small relaxation times [23,32], unlike in Ref. [56] where a large value of the relaxation time was postulated. We check the effect of the initial value of $\Pi(\tau)$ on the evolution by comparing two scenarios: $\Pi(\tau_0) = p(\tau_0)$, which corresponds to an anisotropic momentum (pressure) at the initial time, and $\Pi(\tau_0) = 0$, which corresponds to initially locally equilibrated distributions. With the choice of the relaxation time $\tau_\pi = 6\eta/Ts$, the two initial conditions lead to different results. As before, for each choice of the initial conditions and parameters we retune the parameters of the initial energy density distribution (3.1) to reproduce the final pion rapidity distribution.

In Fig. 11 we show the ratio of the dynamical value of the viscous correction $\Pi(\tau)$ to the Navier-Stokes value of Eq. (6.1). After several fm/c, the stress tensor, which is set initially to zero (dashed-dotted line), relaxes to and overshoots the steady flow value [Eq. (6.1)]. For an initial stress tensor corresponding to the anisotropic effective pressure (solid line), the viscous correction overshoots the Navier-Stokes value almost immediately. Since the dissipative effects are the strongest at the early stages, the integrated entropy production is smaller for an evolution with an initial zero stress tensor than for an evolution starting with a nonzero stress tensor (Fig. 12). Even though, the effect of the change of the initial viscosity correction can be counterbalanced by a suitable change in the initial energy density distribution, the amount of entropy produced in the dynamics depends on the initial value of the dissipative corrections. We also performed a calculation with a smaller relaxation time (dashed lines in Figs. 11 and 12). In that case, the initial value of $\Pi(\tau)$ is less important, as it rapidly relaxes to the steady flow value $\Pi_{\rm NS}(\tau)$. The integrated dissipative effects are smaller.

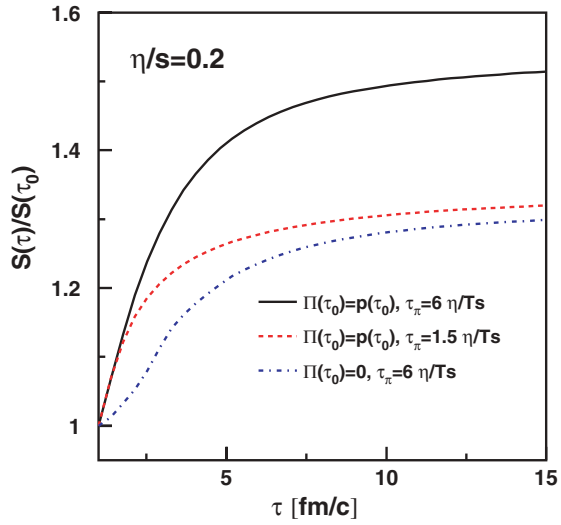

FIG. 12. (Color online) Relative entropy increase in the dissipative evolution at $\eta/s = 0.2$ for two initial conditions for the viscous corrections $\Pi(\tau_0) = p(\tau_0)$ (solid line) and for $\Pi(\tau_0) = 0$ [Eq. (6.1)] (dashed-dotted line), and for a reduced relaxation time $\tau_\pi = 1.5\eta/Ts$ (dashed line).

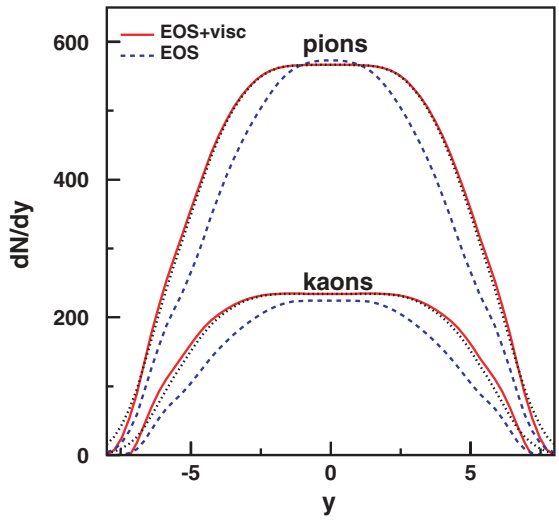

FIG. 13. (Color online) Rapidity distribution of pions (upper curves) and kaons (lower curves, $\times 3$) for LHC plateau-like initial conditions [Eq. (4.5)], calculated for an evolution with shear viscosity coefficient $\eta/s = 0.2$ (solid lines) and for an ideal fluid with a realistic EOS (dashed lines). The dotted line denotes the result of a viscous hydrodynamic evolution, but neglecting the viscous corrections to the particle emission at freeze-out [Eq. (4.3)].

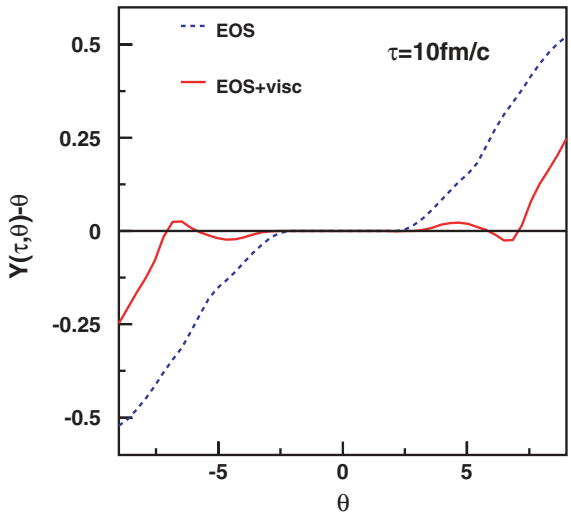

FIG. 14. (Color online) Difference between the flow rapidity of the fluid and the Bjorken value at $\tau = 10$ fm/c, calculated for an evolution with shear viscosity coefficient $\eta/s = 0.2$ (solid line) and for an ideal fluid with a realistic EOS (dashed line) for LHC plateau-like initial conditions.

VII. EXPECTATIONS FOR LHC

In this section we present some simple estimates of the effects of the shear viscosity on the longitudinal expansion at LHC energies. To get a rough estimate, we set arbitrarily the multiplicity of pions for central rapidity at twice the value observed for central collisions at RHIC. The initial energy density distribution in space-time rapidity is modified; it includes a plateau of width σ_p [Eq. (4.5)]. The width of the plateau is $\sigma_p = 3.3$ and takes all the increase of the rapidity range when going from RHIC to LHC energies. The parameter σ is the same as at RHIC energies, and the energy density ϵ_0 is adjusted to reproduce the assumed final pion density $\frac{dN}{dy}|_{y=0}$. The meson distributions are shown in Fig. 13. For the viscous evolution, the plateau in the final meson distributions survives. For an ideal fluid, one gets $\epsilon_0 = 16.9$ GeV/fm^3; while for a shear viscosity $\eta/s = 0.2$, one needs $\epsilon_0 = 12.4$ GeV/fm^3. The difference between the initial energy densities in the viscous and ideal fluid evolutions is not as big as for RHIC energies. At LHC energies, both the ideal and viscous fluid evolutions have a Bjorken scaling form in several units of central rapidity (Fig. 14). The lack of space-time rapidity gradients in the distributions makes the evolution and cooling last longer, around 20 fm/c. Even at freeze-out, the flow is Bjorken-like at central rapidities (Fig. 15). This observation justifies the use at LHC energies of thermal and hydrodynamic models assuming boost invariance [8,57,58]. The hydrodynamic evolution can be restricted to the 1+2 dimensional boost-invariant geometry to describe distributions in the 4–5 central units of rapidity. At the freeze-out hypersurface, dissipative corrections to the momentum distributions have almost disappeared (compare the solid and dotted lines in Fig. 13).

Since the cooling of the fluid due to the longitudinal expansion is slow (like in the Bjorken solution), a realistic modeling of the time scales and of the freeze-out hypersurface must take into account the transverse expansion. The speed of the transverse expansion would determine the lifetime of the system; while at RHIC energies, longitudinal expansion (in space-time rapidity) is also important. We also performed calculations using Gaussian initial energy distributions [Eq. (3.1)] with rescaled width parameters σ for the increased LHC rapidity range. For a viscous fluid, we find a broad region of rapidities where the Bjorken scaling flow survives through the evolution, $|\theta| < 2.5$. For the ideal fluid, the scaling is broken but to a significantly lesser extent than at RHIC energies.

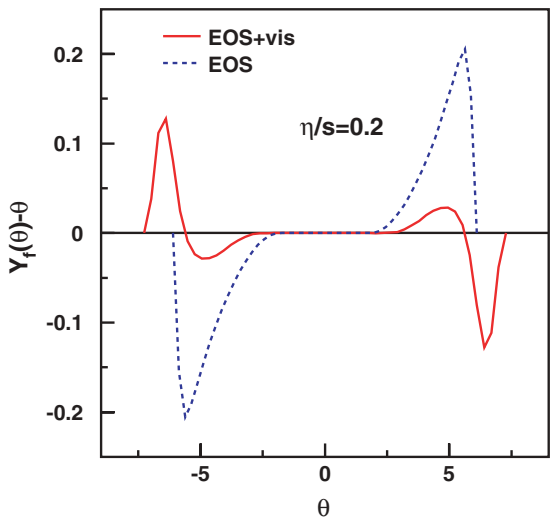

FIG. 15. (Color online) Same as Fig. 14, but calculated at the freeze-out hypersurface.

VIII. CONCLUSIONS

The evolution of a fireball of dense and hot matter created in a heavy-ion collision can be modeled as a hydrodynamic expansion of a viscous fluid. We analyze the effects of the shear viscosity on the longitudinal expansion of the matter. We solve numerically coupled evolution equations for the longitudinal flow, the energy density, and the viscous corrections in a 1+1 dimensional geometry, corresponding to a rapid expansion in the beam direction. As a function of the space-time rapidity, the distribution of matter evolves slowly with proper time. The average density drops and the distribution gets wider. The last phenomenon takes place when the flow of the fluid gets stronger than the Bjorken one. At the freeze-out temperature, the hydrodynamic stage finishes and particles are emitted thermally according to the Cooper-Frye formula. Experimental measurements of the distribution of mesons in rapidity [19] constrain the allowed distribution of the longitudinal velocities of the fluid elements. The correlation between space-time and momentum rapidities of the fluid means that the space-time rapidity extension of the fluid must be limited and that its longitudinal flow cannot deviate significantly from the Bjorken flow. Shear viscosity counteracts the gradients of the velocity field. As a consequence, it slows down the longitudinal expansion. At freeze-out, the energy density distribution in space-time rapidity is narrower and the longitudinal flow gets less accelerated than for the ideal fluid hydrodynamics. Fitting the parameters of a Gaussian initial energy density distribution to reproduce the final meson distributions, one observes a striking effect. With an increasing shear viscosity coefficient, the initial energy density of the fireball decreases significantly, from 16.9 GeV/fm^3 for an ideal fluid to 5.6 GeV/fm^3 for $\eta/s = 0.2$. These estimates cannot be taken literally in a model without transverse expansion, but the qualitative dependence on the shear viscosity coefficient of the longitudinal dynamics is meaningful. Shear viscosity reduces both the cooling and the longitudinal acceleration. In the 1+1 dimensional longitudinal geometry, the fitted energy density corresponds only to an average over the transverse plane. Nevertheless, estimates of the maximal energy density reached in heavy-ion collisions at RHIC energies must be strongly revised down if shear viscosity is effective during the expansion of the fireball. This dramatic reduction of the initial density should also be taken into account in hydrodynamic models dealing with transverse expansion only, both in 1+1 and 1+2 dimensions.

Depending on the balance of the acceleration of the flow from pressure gradients and deceleration from viscosity, the flow gets faster or slower than the Bjorken one. For some values of the parameters, the effects of the shear viscosity and pressure gradients on the longitudinal flow of the fluid cancel, i.e., the flow stays close to the Bjorken flow. This could be an argument justifying models that combine transverse viscous expansion with a Bjorken flow in the beam direction. When the initial conditions are adjusted to reproduce the final meson distributions, we find that the freeze-out hypersurfaces are very similar, irrespective of the value of the shear viscosity coefficient. Obviously the lifetime of the system is not sensitive to viscous effects either (Table II) in the 1+1 dimensional model. At freeze-out, the viscous corrections (from the longitudinal flow) to the thermal distributions are small, except possibly at large space-time rapidities. At LHC energies, a substantial rapidity plateau, where Bjorken scaling applies, is expected to appear. Shear viscosity helps preserve it in a wider rapidity interval through the evolution.

ACKNOWLEDGMENTS

The author is grateful to Mikołaj Chojnacki and Wojtek Florkowski for making available the parametrization of the equation of state. This work was supported by the Polish Ministry of Science and Higher Education under Grant N202 034 32/0918.

[1] P. F. Kolb and U. W. Heinz, in *Quark Gluon Plasma 3*, edited by R. Hwa and X. N. Wang (World Scientific, Singapore, 2004).
[2] P. Huovinen, in *Quark Gluon Plasma 3*, edited by R. Hwa and X. N. Wang (World Scientific, Singapore, 2004).
[3] C. Nonaka, J. Phys. G **34**, S313 (2007).
[4] G. Baym, B. L. Friman, J.-P. Blaizot, M. Soyeur, and W. Czyż, Nucl. Phys. **A407**, 541 (1983).
[5] D. H. Rischke and M. Gyulassy, Nucl. Phys. **A608**, 479 (1996).
[6] M. Kataja, P. V. Ruuskanen, L. D. McLerran, and H. von Gersdorff, Phys. Rev. D **34**, 2755 (1986).
[7] J. Y. Ollitrault, Phys. Rev. D **46**, 229 (1992).
[8] P. F. Kolb, J. Sollfrank, and U. W. Heinz, Phys. Rev. C **62**, 054909 (2000).
[9] P. Huovinen, P. F. Kolb, U. W. Heinz, P. V. Ruuskanen, and S. A. Voloshin, Phys. Lett. **B503**, 58 (2001).
[10] D. Teaney, J. Lauret, and E. V. Shuryak, Phys. Rev. Lett. **86**, 4783 (2001).
[11] C. Nonaka, E. Honda, and S. Muroya, Eur. Phys. J. C **17**, 663 (2000).
[12] T. Hirano and K. Tsuda, Phys. Rev. C **66**, 054905 (2002).
[13] T. Hirano, K. Morita, S. Muroya, and C. Nonaka, Phys. Rev. C **65**, 061902(R) (2002).
[14] J. Adams *et al.* (STAR Collaboration), Phys. Rev. C **71**, 044906 (2005).
[15] S. A. Bass and A. Dumitru, Phys. Rev. C **61**, 064909 (2000).
[16] C. Nonaka and S. A. Bass, Phys. Rev. C **75**, 014902 (2007).
[17] Y. Hama *et al.*, Nucl. Phys. **A774**, 169 (2006).
[18] K. Kajantie, R. Raitio, and P. V. Ruuskanen, Nucl. Phys. **B222**, 152 (1983).
[19] I. G. Bearden *et al.* (BRAHMS Collaboration), Phys. Rev. Lett. **94**, 162301 (2005).
[20] L. M. Satarov, I. N. Mishustin, A. V. Merdeev, and H. Stöcker, Phys. Rev. C **75**, 024903 (2007).
[21] C. E. Aguiar, Y. Hama, T. Kodama, and T. Osada, Nucl. Phys. **A698**, 639 (2002).
[22] H. J. Drescher and Y. Nara, Phys. Rev. C **75**, 034905 (2007).
[23] H. Song and U. W. Heinz, Phys. Lett. **B658**, 279 (2008).
[24] R. A. Lacey *et al.* (2007), arXiv:0708.3512 [nucl-ex].
[25] P. K. Kovtun, D. T. Son, and A. O. Starinets, Phys. Rev. Lett. **94**, 111601 (2005), hep-th/0405231.

[26] R. Venugopalan and M. Prakash, Nucl. Phys. **A546**, 718 (1992).
[27] P. Arnold, G. D. Moore, and L. G. Yaffe, J. High Energy Phys. 11 (2000) 001.
[28] D. Teaney, Phys. Rev. C **68**, 034913 (2003).
[29] R. Baier, P. Romatschke, and U. A. Wiedemann, Nucl. Phys. **A782**, 313 (2007).
[30] R. Baier and P. Romatschke, Eur. Phys. J. C **51**, 677 (2007).
[31] A. K. Chaudhuri, Phys. Rev. C **74**, 044904 (2006).
[32] P. Romatschke, Eur. Phys. J. C **52**, 203 (2007).
[33] T. Hirano, U. W. Heinz, D. Kharzeev, R. Lacey, and Y. Nara, Phys. Lett. **B636**, 299 (2006).
[34] A. Muronga and D. H. Rischke, nucl-th/0407114.
[35] M.-C. Chu, Phys. Rev. D **34**, 2764 (1986).
[36] A. Muronga, Phys. Rev. C **76**, 014909 (2007).
[37] R. Baier, P. Romatschke, and U. A. Wiedemann, Phys. Rev. C **73**, 064903 (2006).
[38] A. Muronga, Phys. Rev. Lett. **88**, 062302 (2002).
[39] W. Israel and J. Stewart, Ann. Phys. (NY) **118**, 341 (1979).
[40] A. Muronga, Phys. Rev. C **69**, 034903 (2004).
[41] A. Muronga, arXiv:0710.3280 [nucl-th].
[42] M. Chojnacki and W. Florkowski, Acta Phys. Pol. B **38**, 3249 (2007).
[43] M. Chojnacki, W. Florkowski, W. Broniowski, and A. Kisiel, arXiv:0712.0947 [nucl-th].
[44] P. Braun-Munzinger, D. Magestro, K. Redlich, and J. Stachel, Phys. Lett. **B518**, 41 (2001).
[45] W. Florkowski, W. Broniowski, and M. Michalec, Acta Phys. Pol. B **B33**, 761 (2002).
[46] F. Cooper and G. Frye, Phys. Rev. D **10**, 186 (1974).
[47] C. Anderlik *et al*., Phys. Rev. C **59**, 3309 (1999).
[48] V. K. Magas, L. P. Csernai, and E. Molnar, Eur. Phys. J. A **31**, 854 (2007).
[49] D. Molnar and P. Huovinen, Phys. Rev. Lett. **94**, 012302 (2005).
[50] J. Adams *et al*. (STAR Collaboration), Phys. Rev. Lett. **90**, 172301 (2003).
[51] P. Bozek, W. Broniowski, and W. Florkowski, Acta Phys. Hung. A. Heavy Ion Phys. **22**, 149 (2005).
[52] S. Cheng *et al*., Phys. Rev. C **69**, 054906 (2004).
[53] G. Torrieri *et al*., Comput. Phys. Commun. **167**, 229 (2005).
[54] H. T. Elze, J. Rafelski, and L. Turko, Phys. Lett. **B506**, 123 (2001).
[55] A. Dumitru, E. Molnar, and Y. Nara, Phys. Rev. C **76**, 024910 (2007).
[56] P. Bozek, arXiv:0711.2889 [nucl-th].
[57] A. Kisiel, T. Taluc, W. Broniowski, and W. Florkowski, Comput. Phys. Commun. **174**, 669 (2006).
[58] N. S. Amelin *et al*., Phys. Rev. C **74**, 064901 (2006).